Werner helicase is a synthetic-lethal vulnerability in Mismatch Repair-Deficient Colorectal Cancer Refractory to Targeted Therapies, Chemotherapy and Immunotherapy

Werner helicase is a synthetic-lethal vulnerability in Mismatch Repair–Deficient Colorectal Cancer Refractory to Targeted Therapies, Chemotherapy and Immunotherapy

AUTHORS

Gabriele Picco[1], Chiara M. Cattaneo[2,5], Esmée J. van Vliet[1], Giovanni Crisafulli[3,4], Giuseppe Rospo[3,4], Sarah Consonni[1,], Sara F. Vieira[1], Iñigo Sánchez Rodríguez[2,5], Carlotta Cancelliere[3], Ruby Banerjee[1], Luuk J. Schipper[2,5], Daniele Oddo[3,4], Krijn K. Dijkstra[2,5], Jindrich Cinatl[6], Martin Michaelis[7], Fengtang Yang[1], Cell Model Network UK Group[1], Federica Di Nicolantonio[3,4], Andrea Sartore-Bianchi[8,9], Salvatore Siena[8,9], Sabrina Arena[3,4], Emile E. Voest[2,5,#], Alberto Bardelli[3,4,#], and Mathew J. Garnett[1,#,*]

1 Wellcome Sanger Institute, Cambridge, UK.

2 Department of Molecular Oncology and Immunology, the Netherlands Cancer Institute, Antoni van Leeuwenhoek Hospital, 1066 CX Amsterdam, the Netherlands

3 Candiolo Cancer Institute, FPO–IRCCS, Candiolo (TO) 10060, Italy.

4 Department of Oncology, University of Torino, Candiolo (TO) 10060, Italy.

5 Oncode Institute, Amsterdam, the Netherlands

6 Institute for Medical Virology, Goethe-University, Frankfurt am Main, Germany

7 School of Biosciences, University of Kent, Canterbury, UK

8 Niguarda Cancer Center, Grande Ospedale Metropolitano Niguarda, Milano, Italy.

9 Dipartimento di Oncologia ed Emato-Oncologia, Università degli Studi di Milano (La Statale), Milano, Italy.

co-senior authors

* corresponding author:

Mathew Garnett

Wellcome Sanger Institute
Cambridge, UK. CB10 1SA
mg12@sanger.ac.uk
Tel: +44 (0)1223 494878

Running Title: Werner helicase is a target in advanced colorectal cancers.

Keywords: Werner helicase, mismatch repair, colorectal cancer, immunotherapy, drug resistance, targeted therapy, chemotherapy.

CONFLICT OF INTEREST STATEMENT

M.J.G. receives research funding from GlaxoSmithKline and is a founder of Mosaic Therapeutics. A.B. is an advisory board member for Roche, Biocartis, Third Rock, Neophore, Phoremost, Illumina and Horizon Discovery. S.A. acted as consultant for MSD Italia. The other authors declare no potential conflicts of interest.

ABSTRACT

Targeted therapies, chemotherapy, and immunotherapy are used to treat patients with mismatch repair-deficient (dMMR)/microsatellite instability-high (MSI-H) colorectal cancer (CRC). The clinical effectiveness of targeted therapy and chemotherapy is limited by resistance and drug toxicities, and about half of immunotherapy patients are refractory to immune checkpoint inhibitors. Loss of Werner syndrome ATP-dependent helicase (WRN) is a synthetic-lethality in dMMR/MSI-H cells. To inform the development of WRN as a therapeutic target, we performed WRN knockout or knockdown in 60 heterogeneous dMMR CRC preclinical models, demonstrating that WRN dependency is an almost universal feature and a robust marker for patient selection. Furthermore, models of resistance to clinically relevant targeted therapy, chemotherapy, and immunotherapy retain WRN dependency. These data show the potential of therapeutically targeting WRN in dMMR/MSI-H CRC patients, and support WRN as a therapeutic option for patients with dMMR/MSI-H cancers refractory to current treatment strategies.

SIGNIFICANCE

We found that a large, diverse set of dMMR/MSI-H CRC preclinical models, including models of treatment refractory disease, are WRN dependent. Our results support WRN as a promising synthetic-lethal target in dMMR/MSI-H CRC tumors as a monotherapy or in combination with targeted agents, chemotherapy or immunotherapy.

INTRODUCTION

DNA mismatch repair (MMR) is an evolutionarily conserved process that recognizes and repairs spontaneously mis-incorporated bases during DNA replication. Microsatellite instability (MSI) is caused by impaired MMR and is a ubiquitous feature in cancer, observed in >20 different tumor types and frequently present in colon, ovarian, endometrial, and gastric cancer, with hundreds of thousands of MSI cancer diagnoses worldwide each year. Lynch syndrome is caused by inherited MMR defects (1). Approximately 10 - 15% of sporadic CRC display dMMR/MSI, with important prognostic and therapeutic implications for patients (2).

Molecularly targeted therapies and chemotherapy agents are used to treat patients with dMMR CRC. Tumor evolution and resistance are major causes of treatment failure and mortality in CRC patients (3,4). For instance, activating KRAS mutations lead to primary and secondary resistance to epidermal growth factor receptor (EGFR)-targeted therapies (5,6). Combination therapies based on vertical suppression of the EGFR - mitogen-activated protein kinase (MAPK) pathway are effective in BRAF-mutated CRC tumors (7–10), but again resistance occurs in preclinical models and the clinical setting (11–13). Rearrangements in *ROS1*, *ALK*, or *NTRK* are also enriched in dMMR tumors (14,15) and lead to hypersensitivity to matched kinase inhibitors (16). Resistance to these matched targeted agents can emerge due to *NTRK1* mutations or by genomic alterations that converge to activate the MAPK pathway (17–19). Immunotherapy with checkpoint inhibitors to PD-1 and PD-L1 are effective against dMMR CRC tumors due to their high mutational burden and increased numbers of neoantigens (20–22). While response rates to checkpoint inhibitors are high and durable for many dMMR CRC patients, around half have primary resistance and are refractory to treatment (22–25), and secondary resistance is a problem (21,26,27). Thus, while advances in precision medicine have led to improved treatment options for dMMR/MSI-H CRC patients, a range of mechanisms can confer resistance and there remains an unmet clinical need for new therapeutic options for patients that are refractory to currently available therapies.

We and others recently identified Werner helicase (WRN) as a synthetic-lethal target in dMMR/MSI-H cancers, with a large proportion of sensitivities in CRC cancer cell lines (28–31). WRN is a member of the RecQ family of DNA helicases and has important but poorly understood roles in maintaining genome stability, DNA repair, replication, transcription, and telomere maintenance (32,33). WRN is selectively essential for dMMR/MSI-H cell viability both *in vitro* and *in vivo*, and WRN knockout in dMMR/MSI-H cells induces double-stranded DNA breaks and widespread genome instability, promoting apoptosis (28–31). A previously unappreciated genetic feature of dMMR/MSI-H cancer cells, DNA $(TA)_n$-dinucleotide repeat expansions, have recently been reported to cause the selective vulnerability to WRN depletion (34). Given these promising results, translational efforts are needed to comprehensively evaluate the efficacy of WRN inactivation and the performance of dMMR/MSI status as a biomarker of response for patient stratification. In this context, targeting WRN potentially represents an effective option as first-line treatment in monotherapy or combinatorial regimens. Additionally, WRN dependency has not been evaluated in advanced or therapy-refractory tumors, such as in the context of primary and acquired resistance to targeted agents, chemotherapy, and/or immunotherapy.

In the present study, we determined the spectrum of WRN dependency in a broad collection of dMMR/MSI-H CRC models, including those derived from patients refractory to targeted agents and chemotherapy, or that displayed limited benefit from immune checkpoint inhibitors. We demonstrate that WRN dependency is widespread in a heterogeneous collection of dMMR models, supporting the use of MSI status for patient stratification. Additionally, we provide evidence that WRN synthetic-lethality is retained in diverse models of primary and acquired resistance to targeted therapy, chemotherapy, and checkpoint inhibitor therapy, expanding the cohort of patients potentially benefiting from WRN-targeted therapies.

RESULTS

WRN dependency in heterogeneous dMMR CRC preclinical models.

WRN helicase is a promising candidate drug target for dMMR cancers. A limited number of CRC cell lines have been used to evaluate WRN inhibition efficacy, and an in-depth evaluation of WRN dependency in a diverse set of preclinical models is missing. To assess the robustness of the WRN-dMMR association, we assembled the largest collection of dMMR CRC preclinical models to date, including 60 unique models (each from a different individual) derived from primary tumors and metastatic lesions, and comprised of both cancer cell lines and newly-generated patient-derived 3D organoid cultures (Fig. 1A and Supplementary Table S1). This collection reflects the genetic/molecular diversity observed in dMMR/MSI-H CRC patients (Supplementary Fig. S1A). Pathogenic missense mutations in KRAS occurred in 35% (n = 21) of models, while BRAF V600E mutations were present in 33% (n=20). Cell lines with oncogenic driver gene fusions in the *NTRK* gene (n = 2), as well as *ALK* and *RSPO3* genes (n = 1 of each), were represented (35,36).

Of the 60 dMMR CRC models, we curated published WRN dependency data for 22 cell lines previously measured by genome-wide CRISPR-Cas9 screens or siRNA-mediated WRN knockdown (28,30,37). Profiles of WRN dependency were generated by CRISPR-Cas9 and/or RNA interference for an additional 38 dMMR CRC preclinical models not included in previous studies, including models derived from metastatic lesions (Fig. 1A). Cell lines (n = 29) were tested by RNA interference (Fig. 1B), while patient-derived organoids (n = 5) were tested by either CRISPR-Cas9-based dropout screening or viability and co-competition assays (Supplementary Fig. S1B-D). Five additional difficult-to-transfect cell lines and models displaying an intermediate response by RNA interference were confirmed

to be sensitive using CRISPR-Cas9-based clonogenic assays (Fig. 1C). Strikingly, altogether 92% (55 of 60) of dMMR/MSI CRC models were dependent on WRN for viability, irrespective of the presence of different cancer driver mutations or gene rearrangements (Fig. 1A). As expected, MMR-proficient models were not affected by WRN knockout (Supplementary Fig. S1B). Interestingly, five outlier dMMR models were not dependent on WRN, retaining >75% viability following depletion (Fig. 1B). We independently confirmed the lack of WRN dependency in these models by CRISPR-Cas9 clonogenic assays and efficient WRN downregulation and knockout by Western Blot (Fig. 1D and Supplementary Fig. S1E-F). Moreover, in WRN-independent MSI-H cells, less than 10% of metaphases are affected by double-strand breaks (DSBs) after WRN knockout, similar to what is detected in MSS cells (Supplementary Fig. S1G-H).

Integration of multiple mutation, gene, and protein expression datasets for the models confirmed that all had one or more alterations in a gene encoding a protein involved in MMR (Fig. 1E). WRN dependency was not associated with mutational burden ($p = 0.88$; Student's t-test). Interestingly, we observed a statistically significant enrichment for MSH2 ($p = 0.0048$ or 0.0357 excluding cell lines with missing data; Fisher's exact test) and MLH1 ($p = 0.0096$ or 0.0625) alterations in WRN-dependent versus independent cell models. We re-assessed MSI status by PCR and independently evaluated MLH1, MSH2, and MSH6 protein expression by Western Blot for WRN independent lines (Supplementary Fig. S2A). All the models were confirmed MSI-H except GEO, which was re-classified as MSI-low, explaining WRN independence and the absence of alterations in canonical MMR pathway genes in this model. An analogous analysis in an independent set of cancer models from non-CRC dMMR/MSI-H-predominant tissue lineages confirmed an enrichment for MSH2 alterations (p-value = 0.0391) in WRN dependent models, but not MLH1 (Supplementary Fig. S2B). We then performed PCR-based and WGS sequencing coverage analysis to assess MSI cell lines for expanded TA-repeats, a recently identified feature of MSI cells contributing to WRN synthetic-lethality (34). WGS sequencing data were available for a subset of cell lines. We confirmed the presence of expanded TA-repeats in MSI WRN-dependent cell lines compared to MSS cells, as evidenced by a failure to PCR amplify some broken repeat regions and reduced WGS sequencing coverage across broken repeats (p-value < 0.001) (Supplementary Fig. S2C-D). Strikingly, MSI-H WRN-independent cells were most similar to MSS cells, with little or no evidence of expanded TA-repeats with either analysis. The expanded TA-repeat phenotype was variable in cell lines within the MSI subgroups, but nonetheless our results suggest that repeat length is not altered, or at least not to the same extent, in WRN-independent MSI-H cell lines.

Overall, employing a heterogeneous collection of dMMR/MSI-H CRC models, including a large cohort of previously untested models, our results indicate that inhibiting WRN has a nearly universal synthetic-lethal effect, strongly supporting WRN as a target and dMMR as a therapeutic biomarker for patient selection. There exists however a rare subset of dMMR/MSI-H CRC, characterised by the absence of MLH1 and MSH2 alterations and expanded TA-repeat phenotype, which are not dependent on WRN and would presumably be refractory to WRN targeted therapies.

WRN inhibition is effective in dMMR CRC models of acquired resistance to targeted therapies and chemotherapy

New treatment options for patients with advanced and treatment-refractory disease represents an unmet clinical need. Given the diverse genetic background of tumors dependent on WRN, we hypothesized that dMMR tumors with acquired resistance to targeted therapies and chemotherapy may retain WRN dependency. To investigate this, we began by using isogenic dMMR CRC cell models of acquired resistance to clinically-relevant single agent or combination therapies (Fig. 2A) (11,18,38). Specifically, cells were made resistant *in vitro* to the anti-EGFR monoclonal antibody cetuximab, the combination of cetuximab and the BRAF inhibitor (BRAFi) dabrafenib (D+C), or the NTRK inhibitor entrectinib. We confirmed drug sensitivity of the parental cell lines and corresponding resistance of the derivative line (Supplementary Fig. S3A). Upon RNAi-mediated silencing of WRN, all models showed a marked reduction in fitness (Fig. 2B). To confirm these results, we independently performed CRISPR-Cas9 knockout of WRN and observed a marked reduction in cell fitness in all drug-sensitive and drug-resistant lines (Fig. 2C). Downregulation or knockout of the WRN protein was confirmed by Western blot (Supplementary Fig. S3B-C).

Triple therapy based on EGFR, BRAF, and MEK inhibitors recently demonstrated efficacy in metastatic CRC patients with the BRAF V600E mutation (9). To validate WRN dependency in this setting, we selected drug-resistant BRAF-mutated VACO432 cells in the presence of dabrafenib and cetuximab (D+C) double therapy, and dabrafenib, trametinib, and cetuximab (D+C+T) triple therapy (Fig. 2A). The resulting resistant cells had a KRAS G13D mutation, which is a common mechanism of acquired resistance to this therapy regimen in CRC patients (10) (Supplementary Fig. S3D). Remarkably, cell lines resistant to double or triple therapy retained notable sensitivity to the loss of WRN (Fig. 2B-C). Lastly, we used cell lines derived from a patient-derived xenograft (PDX) model generated from a CRC patient positive for *LMNA-NTRK1* rearrangement, treated *in vivo* with entrectinib in a mouse-human co-clinical trial (18). An NTRK1 G595R mutation led to entrectinib resistance

both in the patient and in the resistant cell line generated from the tumor that acquired resistance *in vivo* (Supplementary Fig. S3E-F). Again, both the entrectinib-sensitive and resistant cell lines showed a strong dependency on WRN (Fig. 2D-F). WRN knockout in LMNA-NTRK1 cells led to numerous chromosomal abnormalities, including chromatid and chromosome breaks and rearrangements (Fig. 2G-H and Supplementary Fig. S3G).

We next evaluated WRN dependency in the setting of acquired resistance to standard of care chemotherapeutic agents. We treated the MSI CRC cell line HCT116 with increasing doses of oxaliplatin (two independent selections) until resistant cells emerged. We also generated MSI CRC SW48, RKO and LoVo cells resistant to irinotecan, oxaliplatin, or 5-FU (Fig. 3A-B and Supplementary Fig. S4A). Additionally, we established a cell line (IRCC-114-XL) from the PDX of a patient with a clinical history of Lynch syndrome, who relapsed after surgery and 6 months of treatment with mFOLFOX (folinic acid, 5-fluorouracil, and oxaliplatin), displaying no objective response and rapid progression of disease (Fig. 3C-D). Notably, WRN knockout or depletion markedly reduced the viability of all twelve chemotherapy-resistant dMMR/MSI-H CRC sublines, and IRCC-114-XL cells (Fig. 3E-H, Supplementary Fig. S4B-D). WRN knockout in IRCC-114-XL cells promoted DSBs formation and marked chromosomal defects (Fig. 3I-J and Supplementary Fig. S4E-G).

These results demonstrate that dMMR CRC cells resistant to clinically-relevant targeted therapies or chemotherapy retain a synthetic-lethal dependency on WRN, irrespective of the mutational background of the tumor and the therapeutic regimen to which resistance was acquired.

Patient-Derived dMMR CRC Models Refractory to Immunotherapy are WRN Dependent

We next used multiple patient-derived organoid models to investigate whether dMMR CRC tumors responding poorly to immunotherapy are dependent on WRN. First, we evaluated WRN dependency in the setting of resistance to T cell-mediated tumor cell killing using an autologous tumor organoid and peripheral blood lymphocyte co-culture system (39,40). We made use of a previously established organoid model from a dMMR CRC patient (CRC-12) together with matched tumor-reactive T cells generated by two weeks of co-culturing peripheral blood mononuclear cell (PBMCs) with tumor organoids (39) (Fig. 4A left panel). CRC-12 cells were killed by autologous tumor-reactive T cells in a dose-dependent manner. Killing was rescued by the addition of a MHC class I blocking antibody, confirming an antigen-specific CD8+ T cell mediated response (Supplementary Fig. S5A). To generate a model of resistance, we *in vitro* selected a sub-population of CRC-12 organoids resistant to T cell killing (CRC-12-RES). In addition, as a positive control for

resistance, we knocked out the *B2M* gene to create an isogenic CRC-12 line (CRC-12-B2M), and confirmed loss of MHC-I expression (Supplementary Fig. S5B). CD137 surface expression was used as a marker for T cell activation. Autologous CD8+ T cells were reactive to CRC-12 tumor organoids, whereas no CD8-mediated reactivity was detected in the presence of CRC-12-RES or CRC-12-B2M organoids; CD4+ T cell reactivity remained unaffected (Fig. 4B and Supplementary Fig. S5C-D). Accordingly, while CRC-12 parental organoids were killed by autologous tumor-reactive T cells, CRC-12-RES and CRC-12-B2M KO organoids were unaffected by the presence of the reactive population (Fig. 4C). Resistance in CRC-12-RES organoids was not due to the loss of MHC-I or IFNγ receptor (Supplementary Fig. S5B and E), and B2M mutations were absent. Next, we used these advanced models to investigate WRN dependency. Strikingly, WRN knockout inhibited viability in the parental CRC-12 organoid, as well as CRC-12-RES, demonstrating that strong WRN dependency is retained in a model refractory to autologous T cell-mediated cytotoxicity (Fig. 4D).

To corroborate our findings, we investigated WRN dependency in two organoids derived from a sporadic dMMR CRC patient with variable clinical response to immunotherapy. CRC-14a and CRC-14b were derived from biopsies obtained from a peritoneal metastasis and primary tumor of a patient with a clinical treatment history of capecitabine, oxaliplatin, and bevacizumab, then treated with nivolumab monotherapy (Fig. 4A, right panel). The CRC-14a metastasis biopsy was taken before the start of the checkpoint blockade, and this lesion regressed on nivolumab, whereas the biopsy for CRC-14b was taken from the primary tumor upon progression on nivolumab (Fig. 4E). To induce (or enrich for) a tumor reactive T cell population, both organoids were individually co-cultured with autologous PBMCs obtained before treatment with nivolumab (39,40). After 2 weeks of co-culture with CRC-14a (from the responsive metastatic lesion), we observed marked and selective CD8+ T cell reactivity against CRC-14a (but not CRC-14b) organoids (Fig. 4F). In contrast, when CRC-14b organoids (derived from the non-responding primary tumor) were used in the co-culture, no T cell reactivity was detected against any of the organoid lines. Of note, CD4+ T cell reactivity remained unaltered (Supplementary Fig. S5F). Interestingly, loss of MHC-I expression was found in CRC-14b, potentially explaining the failure to generate tumor reactive T cells from PBMCs, and lack of clinical response to nivolumab treatment (Supplementary Fig. S5G). B2M protein expression in CRC-14b was confirmed by flow cytometry (Supplementary Fig. S5H) and no frameshift or nonsense mutations were detected, suggestive of a B2M-independent resistance mechanism, although a non-synonymous variant of unknown significance (Y30C) was present. These results support CRC-14b as an ex vivo model to evaluate WRN dependency in an immune refractory

setting. Viability assays after CRISPR-based knock-out of WRN in CRC-14b organoids revealed a strong dependency on the WRN helicase (Fig. 4G-H).

Altogether, these data provide multiple lines of evidence that WRN dependency is retained in patient-derived dMMR CRC preclinical models of resistance to immunotherapy.

DISCUSSION

We have investigated the potential of therapeutically targeting WRN in preclinical models of dMMR CRC, including in the setting of resistance to targeted therapies, chemotherapy and immunotherapy. We used the largest collection of dMMR CRC preclinical models characterized to date, nearly tripling the number assessed for WRN dependency. Greater than 90% of models were WRN dependent, including models with diverse genetic backgrounds, molecular contexts, and oncogenic alterations, suggesting WRN dependency is an almost universal feature of dMMR/MSI CRC cells. This reinforces dMMR/MSI status as a robust biomarker for WRN synthetic-lethality and to stratify patients for the clinical development of WRN-targeted therapies. Notably, for the ~7% of dMMR CRC models that were WRN-independent, functional expression of MSH2 and MLH1 was retained, suggesting that WRN dependency is influenced by the underlying MMR-pathway genes altered. Moreover, TA-repeats are differentially altered compared to MSI-H WRN-dependent lines, suggesting that loss of MSH2 or MLH1 might be of particular importance to generate TA-dinucleotide repeat expansions reported to confer WRN addiction (34). This observation warrants confirmation in larger cohorts but, if validated, could provide mechanistic insight into the WRN-MSI synthetic lethal interaction and help refine patient selection strategies based on novel biomarkers of sensitivity.

Inhibition of WRN leads to genome instability in dMMR cells. This may be due to a catastrophic failure to process TA-dinucleotide expansions that accumulate in MSI cells (34). This is distinctive from targeted agents which inhibit specific oncogenic alterations in cancer cells and immunotherapies which suppress immune evasion and tolerance. Consistent with an orthogonal therapeutic activity, WRN is a synthetic-lethality in preclinical models of resistance to molecular targeted therapies, including models addicted to a diverse set of oncogenic alterations and that acquire different genetic mutations to promote therapy escape. In addition, WRN is synthetic-lethal in patient-derived models from dMMR CRC patients with limited clinical benefit from chemotherapy and PD-1 inhibitors, or resistant to autologous T-cell mediated cancer cell killing. Resistance to targeted therapies can occur through a range of mechanisms, including through reactivation of the targeted pathway,

while for immunotherapies, several mechanisms of resistance are emerging including loss of antigen processing and presentation (41). Our finding suggests that WRN inhibitors could be effective as a second or third-line monotherapy for dMMR patients. Indeed, WRN sensitivity was not correlated with mutational load in dMMR tumors, whereas low mutability in dMMR tumors is negatively associated with response to immune checkpoint blockade (25,42). Because of their independent modes of action, combining a checkpoint inhibitor, chemotherapy or a targeted therapy with a WRN inhibitor may suppress cross-resistance and promote tumor eradication. Moreover, WRN inhibition may also be synergic with immunotherapy as loss of DNA repair modulates the neoantigen landscape and increases mutational burden, leading to an enhanced immune response (43). DNA damage resulting from loss of WRN could likewise potentiate the effects of immunotherapy, similar to combining chemotherapeutics with immune-modulating agents (44). Investigations into the effects of WRN inhibition on immune recognition and surveillance to increase therapeutic efficacy for patients with dMMR CRC refractory to immunotherapy regimens are warranted. Collectively, our findings provide a rationale for the clinical development of WRN-targeted medicines in advanced CRC patients, and potentially in combination with existing therapies.

For our study, we exploited a tumor organoid T cell co-culture system as a preclinical tool to assess WRN dependence. We used for the first time an organoid co-culture system to model *in vitro* acquired resistance to T cell killing. Mechanisms driving resistance to immunotherapy and tumor reactive T-cells in these model are currently unverified, but loss of MHC-I expression in organoids derived from an anti-PD-1 resistant tumor points to a loss of antigenicity and immunogenicity due to immune selection pressure, favouring the growth of tumor cell clones with a non-immunogenic phenotype, similar to what has been described clinically (45).

WRN has a role in maintenance of genome stability and Werner syndrome is an autosomal recessive disorder associated with premature ageing caused by mutation in the WRN gene. Nonetheless, WRN mutations are compatible with human development well into the fourth decade of life, and disease-associated complications take decades to manifest, suggesting a therapeutic window of activity could be achieved using WRN-targeted medicines in appropriately selected patients. WRN is the focus of ongoing drug discovery programs. Small molecule WRN helicase inhibitors have been reported (46,47), but their efficacy is impaired by lack of selectivity against dMMR cells, off-target effects, and cytotoxicity to normal cells (48). Our study provides new information to support the continued development of WRN-targeted medicines. Furthermore, as potent and selective WRN drugs are developed, our findings will inform patient selection strategies and provide a strong

rationale for their clinical development in patients with dMMR tumors not benefiting from current therapeutics alone.

METHODS

Cell models

A full description of cell models (cell lines and organoids) used in this study is provided in Supplementary Table 1. The majority of cell lines were curated from the Genomics of Drug Sensitivity 1000 cell line collection and are annotated in the Cell Model Passports database (https://cellmodelpassports.sanger.ac.uk/) (49), or are from previously reported collection (35,50). The LIM1215 parental cell line has been described previously (51) and was obtained together with LIM2405, LIM2412 and LIM2537 from Prof. Robert Whitehead, Vanderbilt University, Nashville, with permission from the Ludwig Institute for Cancer Research, Zurich, Switzerland. LIM2550 and LIM2551 were obtained from CellBank Australia. Cell lines were maintained in their original culturing conditions according to supplier guidelines or as previously described (52). Cells were supplemented with 10% FBS, 2 mM L-glutamine, and antibiotics (100 U/mL penicillin and 100 mg/mL streptomycin) and grown at 37 °C and 5% CO2 air incubator. Cells were routinely screened for the absence of mycoplasma contamination using the Venor®GeM Classic kit (Minerva Biolabs). The identity of each cell line was checked before starting each experiment and after every genomic DNA extraction by PowerPlex® 16 HS System (Promega), through Short Tandem Repeats (STR) at 16 different loci (D5S818, D13S317, D7S820, D16S539, D21S11, vWA, TH01, TPOX, CSF1PO, D18S51, D3S1358, D8S1179, FGA, Penta D, Penta E, and amelogenin). Amplicons from multiplex PCRs were separated by capillary electrophoresis (3730 DNA Analyzer, Applied Biosystems) and analyzed using GeneMapper v 3.7 software (Life Technologies). The MSI status of the cell lines and organoids in Fig. 1 was previously reported (35,39,53) and/or publicly available (Cell Model Passports database (https://cellmodelpassports.sanger.ac.uk/) (49). The PDX-derived cell line IRCC-114-XL was generated following previously described procedures (37) approved by the Italian Ministry of the Health and the Local Ethics Committee (Protocol n. 1014/2009 and 194/2010 of Grande Ospedale Metropolitano Niguarda, Milano, Italy) in accordance with generally accepted guidelines for the use of human material. Organoids were derived at the Sanger Institute by the Cell Model Network UK consortium (CMN-UK) as part of the Human Cancer Model Initiative (HCMI), and genomic characteristics, such as microsatellite stability status, were downloaded from the Cell Model Passports website (49).

Patient-derived organoids for immuno-oncology studies were derived at the Netherlands Cancer Institute as previously reported (39,40). Briefly, tumor tissue was mechanically dissociated and digested with 1.5 mg/mL of collagenase II (Sigma-Aldrich),10 µg/mL of hyaluronidase type IV (Sigma-Aldrich), and 10 µM Y-27632 (Sigma-Aldrich). Cells were

embedded in Geltrex (Geltrex LDEV-free reduced growth factor basement membrane extract, Gibco) and placed in a 37 °C incubator for 20 min. Human CRC organoids medium is composed of Ad-DF+++ (Advanced DMEM/F12 (GIBCO) supplemented with 2 mM Ultraglutamine I (Lonza), 10 mM HEPES (GIBCO), and 100/100 U/mL Penicillin/Streptomycin (GIBCO), 10% Noggin-conditioned medium, 20% R-spondin1-conditioned medium, 1x B27 supplement without vitamin A (GIBCO), 1.25 mM N-acetylcysteine (Sigma-Aldrich), 10 mM nicotinamide (Sigma-Aldrich), 50 ng/mL human recombinant EGF (Peprotech), 500 nM A83-01 (Tocris), 3 μM SB202190 (Cayman Chemicals) and 10 nM prostaglandin E2 (Cayman Chemicals). Organoids were passaged every 1–2 weeks by incubating in TrypLE Express (Gibco) for 5–10 min followed by embedding in Geltrex. Organoids and cell lines were authenticated by SNP array and regularly tested for Mycoplasma using Mycoplasma PCR43 and the MycoAlert Mycoplasma Detection Kit (catalog no. LT07-318). In the first two weeks of organoid culture, 1x Primocin (Invivogen) was added to prevent microbial contamination. All the procedures performed with patient specimens were conducted under the approval of the institutions' local Ethical Committee, after the written informed consent of the patients. The study (NL48824.031.14) was approved by the Medical Ethical Committee of the Netherlands Cancer Institute – Antoni van Leeuwenhoek hospital and written informed consent was obtained from all patients. Peripheral blood and tumor tissue were obtained from patients with a confirmed diagnosis of colorectal cancer.

Generation of subline resistant to chemotherapy.

Colorectal cancer cell lines SW48, LoVo, RKO and HCT116 were obtained from ATCC. SW48, LoVo and RKO drug-resistant sublines were derived from the resistant cancer cell line (RCCL) collection (https://research.kent.ac.uk/industrial-biotechnology-centre/the-resistant-cancer-cell-line-rccl-collection/) (54) and established by continuous exposure to stepwise increasing drug concentrations as previously described (55). SW48, LoVo and RKO resistant sublines were adapted to growth in the presence of 5-fluorouracil (5-FU) (8, 1.5 and 3μM; 5f-R), irinotecan (8, 0.34 and 1.7 μM; ir-R), or oxaliplatin (5, 5 and 3.8 μM; ox-R), respectively. SW48, LoVo and RKO cells were propagated in DMEM/F-12 supplemented with 10 % FBS, 100 IU/mL penicillin and 100 μg/mL streptomycin at 37°C. Similarly, HCT116 resistant sublines (HCT116 ox-R_A and B) were adapted to growth in the presence of 5 μM of oxaliplatin.

Molecular characterization of dMMR cancer cell lines

The MSI status of WRN independent dMMR models (GEO, HCT15, HDC143, SNU175, and IRCC3HL) was re-assessed and confirmed with the MSI Analysis System kit (Promega). The analysis requires a multiplex amplification of seven markers, including five mononucleotide repeat markers (BAT-25, BAT-26, NR-21, NR-24, and MONO-27) and two pentanucleotide repeat markers (Penta C and Penta D). The products were analyzed by capillary electrophoresis in a single injection (3730 DNA Analyzer, ABI capillary electrophoresis system (Applied Biosystems). Results were analyzed using GeneMapper V5.0 software. Mutations in MMR-pathway genes were downloaded from The Cell Model Passport or Dependency Map (DepMap) websites. Mutations in IRCC3-HL and HDC143 cell lines were obtained by whole-exome sequencing data generated at the Candiolo Cancer Institute. Mutational burden of cancer cell lines was computed analyzing NGS data previously published (56–58) and available at the European Nucleotide Archive (ENA; accession codes PRJEB33045 and PRJEB33640). Genetic analysis was performed as previously described (56–58). Mutations in VACO432 C+D+T cell model were detected through Sequenom analysis by using Myriapod® Colon status kit (Diatech Pharmacogenetics, Italy). SNP were excluded except if predicted as damaging. For gene expression, we used RNAseq (RPKM) data previously generated (59). For GEO and HDC143 we used gene expression data obtained previously (35). Proteomics data were already available (60,61). To identify which MMR-pathway gene displayed altered gene or protein expression, we computed the Z-score by gene across all the cell lines in the respective dataset and considered genes with Z-score or normalized values less than negative 2 to identify genes downregulated in a particular sample. WRN dependency was obtained mining essentiality data obtained from multiple sources: Project Score (https://score.depmap.sanger.ac.uk/) and Dependency Map (DepMap; https://depmap.org/portal/) websites or additionally available datasets (62). Cell lines were considered WRN dependent if WRN essentiality reached threshold values of significance in at least one of the CRISPR (Sanger or DepMap Public 20Q2) or combined RNAi (Broad, Novartis, Marcotte) datasets. Statistical significance was computed by performing Fisher's exact comparison for the presence of cumulative alterations (mutation, gene expression, and protein expression) detected in WRN-dependent versus WRN-independent cell lines. For TA-dinucleotide repeat expansion analysis whole genome sequencing data for cancer cell lines were downloaded from SRA study SRP186687 (https://trace.ncbi.nlm.nih.gov/Traces/study/?acc=SRP186687). Whole genome sequencing data for IRCC3_XL, HDC143 and SNU175 are available at the European Nucleotide Archive (ENA; accession code PRJEB43711). Fastq files were mapped to human genome reference GRCh38 using bwa-mem alignment algorithm (http://arxiv.org/abs/1303.3997) and then PCR duplicates were marked using MarkDuplicates tool (http://broadinstitute.github.io/picard). The genomic coordinates of broken and unbroken regions were downloaded from

Wietmarschen et al. Nature, 2020 (34), and then converted into the GRCh38 assembly version using the LiftOver tool (63). A total of 5362 and 59926 broken and unbroken regions were analysed, respectively. For all WGS the fragments per base per million (FPBM) were calculated in each interval as reported in Wietmarschen et al. Nature, 2020 (34), and, lastly, the median values of broken and unbroken regions were estimated in each sample. PCR-based analysis of TA-repeats were performed as previously reported (34), using the same PCR primer sequences. Samples were denatured at 95 °C for 3 min and underwent 28 cycles of denaturation at 95 °C for 30s, annealing/extension at 60 °C for 3 min, followed by an extension at 60 °C for 10 min. PCR products were separated on a 2% agarose gel and visualized by ethidium bromide staining.

Immunohistochemistry

Immunohistochemistry assessment of MMR status in patient-derived organoids derived at the Netherlands Cancer Institute was performed as follows. Formalin-fixed, paraffin-embedded (FFPE) sections were obtained from both pretreatment biopsies and resection specimens. Baseline tumor biopsies were used to assess MMR status using IHC for MLH1, PMS2, MSH2 and MSH6 according to standard protocols for the Ventana automated immunostainer (MLH1 Ready-to-Use, M1, 6472966001, lot no. G07286, Roche; MSH2, Ready-to-Use, G219-1129, 5269270001, lot no. 1616008C, Roche; MSH6, 1/50 dilution, EP49, AC-0047, lot no. EN020910, Abcam; PMS2, 1/40 dilution, EP51, M3647, lot no. 1012289, Agilent Technologies).

Generation of Cas9 expressing cell lines

Between 2-3 x 10^5 cells were transduced overnight with lentivirus containing Cas9 (Addgene, 68343) in a T25 flask, in the presence of polybrene (8 µg/mL). Lentivirus-containing medium was refreshed the following day with complete medium. Tumoral organoids were dissociated into single cells and incubated overnight in suspension and complete media. The following day cells were seeded in matrigel and grown as organoids. Positively transduced cells were selected for with blasticidin (20 µg/mL, Thermo Fisher Scientific, A1113903) starting 48 hours after transduction. Cas9 activity was determined as described previously (30). Briefly, cells or organoids were transduced with Cas9 reporter virus (pKLV2-U6gRNA(gGFP)- PGKBFP2AGFP-W), as described above. The number of BFP+ and GFP-BFP double-positive cells were determined by flow cytometry on a BD LSR Fortessa instrument (BD), and data were subsequently analysed using FlowJo to determine the percentage of BFP+ cells. All cell lines and organoid lines displayed Cas9 activity over 75%.

Organoid genome editing and genome-wide CRISPR-Cas9 screens

The genome-wide sgRNA library transduction was adapted from a previous protocol recently reported to screen cancer cell lines (30). Briefly, tumor organoids were dissociated into single cells, and a total of $3.3x10^7$ cells were transduced overnight, in suspension, with an appropriate volume of the lentiviral-packaged whole-genome sgRNA library to achieve 30% transduction efficiency (100x library coverage) and polybrene (8 µg/mL). The following day, cells were seeded in matrigel and grown as organoids. After 48h organoids were selected with Puromycin (2 µg/mL). After 14 days, approximately $2x10^7$ cells were collected, pelleted and stored at −80 °C for DNA extraction. Genomic DNA was extracted using the Qiagen, Blood & Cell Culture DNA Maxi Kit, 13362, as per the manufacturer's instructions. PCR amplification, Illumina sequencing (19-bp single-end sequencing with custom primers on the HiSeq2000 v.4 platform) and sgRNA counting were performed as described previously (30).

To generate B2M knockout organoids lines, we used sgRNA targeting B2M (GGCCGAGATGTCTCGCTCCG), cloned into LentiCRISPR v2 plasmid and the virus was produced by standard method. To express luciferase in the organoids, we used pLenti CMV Puro LUC (w168-1) (Plasmid #17477; Addgene).

CRISPR-Cas9 viability and co-competition assay

Approximately 1.5-3 x 10^3 Cas9 expressing cells per well, of a 96-well plate were transduced overnight in the presence of polybrene (8 µg/mL) with lentiviral constructs containing sgRNAs against a non-essential gene (CYP2A13, GTCACCGTGCGTGCCCCGG), an essential gene (PLK1, GCGGACGCGGACACCAAGG), and two sgRNAs against WRN (#1, GAGCATGAGTCTATCAGAT and #2, GTCCTGTGGAACATACCATG). Medium was refreshed for fresh complete medium the following day, and cells were treated with blasticidin (20 µg/mL) and puromycin (2 µg/mL, Thermo Fisher Scientific, A1113803) to select for Cas9 expressing cells carrying the sgRNAs. Cells were allowed to grow for approximately 7-10 days before cell viability was determined using the CellTiter-Glo 2.0 Assay (Promega, G9241). For the co-competition assay, organoids were transduced as above to achieve 50% of BFP-positive cells and seeded in six-well plates the day after to form organoids. A co-competition score was determined as the ratio of the percentage of BFP-positive (sgRNA trasduced) cells on day 14 compared to day 3, as measured by flow cytometry.

RNA interference-based sensitivity assay

Approximately 1.5-3.5 x 10^3 cells per well, of a 96-well plate, were reverse transfected with ON-TARGETplus siRNA, to a final concentration of 20 nM, using RNAiMAX (Invitrogen) as per manufacturer instructions. Each experiment included transfection reagent only as mock control, a non-targeting pool as negative control (Dharmacon, D-001810-10-05), polo-like kinase 1 (PLK1) pool as positive control (Dharmacon, L-003290-00-0010), and the targeting pool against WRN (Dharmacon, L-010378-00-0005). siRNA sequences: Non-targeting Control Pool (UGGUUUACAUGUCGACUAA, UGGUUUACAUGUUGUGUGA, UGGUUUACAUGUUUUCUGA, UGGUUUACAUGUUUUCCUA), PLK1 (GCACAUACCGCCUGAGUCU, CCACCAAGGUUUUCGAUUG, GCUCUUCAAUGACUCAACA, UCUCAAGGCCUCCUAAUAG), WRN (GAUCCAUUGUGUAUAGUUA, GCACCAAAGAGCAUUGUUA, AUACGUAACUCCAGAAUAC, GAGGGUUUCUAUCUUACUA). Cells were grown for 5-7 days. Cell viability was assessed using the CellTiter-Glo 2.0 Assay (Promega, G9241) as described below.

Drug sensitivity assay

Drug sensitivity assays were performed to confirm the resistance of each cell line. For each pair of cell lines of interest, approximately 1.5-2.5 x 10^3 cells per well of a 96-well plate were seeded and grown for both the drug-sensitive and drug-resistant lines. The following day, a concentration range of the respective drug was added to the cells, in triplicate per concentration per line, and cells were allowed to grow for 7-10 days. Cell viability was assessed using the CellTiter-Glo 2.0 Assay (Promega, G9241).

Cell viability assay

Cell viability was determined using the CellTiter-Glo 2.0 Assay (Promega, G9241), as per manufacturer instructions. Briefly, 25 µL of Celltiter-Glo 2.0 reagent was added to each well of a 96 well plate and incubated for at least 20 minutes at room temperature in the dark. After incubation, the luminescent signal was read out using an Envision Multiplate Reader.

Western blotting

Western blotting was performed to confirm the absence of WRN in siRNA and CRISPR treated cells. For siRNA-based knockdown, approximately 0.5-1 x 10^6 cells were seeded in a 6-well plate in OptiMem and treated as described above. This assay included siRNA pools targeting WRN and a non-targeting pool as negative control. For CRISPR-based knockdown, approximately 1 x 10^6 cells were seeded in a 10cm cell culture dish and treated as described above. This assay included two sgRNAs against WRN and a negative control

without virus. Protein was isolated 72-96h after seeding with 100-150 uL RIPA buffer supplemented with proteinase and phosphatase inhibitors. Lysate concentration was determined using the BCA Assay. Per sample, 20-30 µg of lysate was loaded onto a 4-12 % Bis-Tris gel (Invitrogen) for SDS-PAGE followed by protein transfer from the gel onto a PVDF membrane. Membranes were blocked in 5% milk (in TBST) and incubated overnight with the appropriate antibodies. Blots were washed in TBST and incubated with secondary antibody for 1h at room temperature. Blots were washed in TBST before the signal was enhanced with Super Signal Dura and visualized. The following primary antibodies were used for immunoblot analysis: anti-WRN antibody (Cell Signalling Technologies, 4666, 1:2000), and anti-β-tubulin (Sigma-Aldrich, T4026: 1:5000) as loading control. Anti-Mouse IgG HRP-linked secondary antibody (GE Healthcare, #NA931) was used as a secondary antibody. Precision Plus Protein Standards (BioRad, 161-0373) was used as a molecular weight marker.

Karyotype analysis with human M-FISH (multiplex fluorescence in situ hybridisation) probes.

WRN was knocked out using CRISPR-Cas9 as described above. Puromycin selection (2 µg/mL) was initiated 48h after transduction, and cells were harvested for metaphases 96h after transduction from control and WRN knockout cell lines followed a standard protocol with modifications. Briefly, cells growing in T150 flasks were treated with colcemid (KaryoMaxTM ColcemidTM Solution in PBS, 10 g/mL, ThermoFisher Scientific), to a final concentration of 0.1 g/mL for 1.5h. TrypLE Express Enzyme (ThermoFisher Scientific) was used to dissociate adherent cells to obtain a single cell suspension, which was pelleted down and resuspened in a hypotonic solution (0.56% KCl in H2O) for 12 -14 minutes and subsequently fixed with Carnoy's fixative, 3:1 (v/v) methanol: acetic acid. FISH analysis was performed as previously reported (64). Metaphase slides were prepared and fixed in acetone (Sigma Aldrich) for 10 min followed by baking at 62°C for 30 min. Denaturation of metaphase spreads was carried out by immersing slides in an alkaline denaturation solution (0.5 M NaOH,1.0 M NaCl) for 7 ½ - 8 minutes followed by two subsequent washes in 1 M Tris-HCl (pH 7.4) and 1×PBS, 4 min each. Slides were dehydrated in a 70%, 90% and 100% ethanol series. The probe mix (24 colour human M-FISH paint) was denatured at 65°C for 10 min before applying onto the denatured slide. Hybridisation was carried out at 37°C for two nights. Post hybridisation steps included a 30 min (approx.) wash in 2×SSC at 37°C, to remove coverslips, followed by a 5 min stringent wash in 0.5×SSC at 75°C, a 5 min rinse in 2×SSC containing (0.05% Tween-20 (VWR) and another 5 min rinse in 1×PBS, both at room temperature. Slides were finally mounted in Vectashield® VibranceTM Antifade Mounting

medium with DAPI (4', 6-diamidino-2-phenylindole), Vector Laboratories. Metaphases were imaged using AxioImager D1 microscope equipped with appropriate narrow-band pass filters for DAPI, Aqua, FITC, Cy3, Texas Red and Cy5 fluorescence. Digital images were captured using the SmartCapture software (Digital Scientific, UK) and 20 randomly selected metaphase cells were karyotyped and analysed with particular interest in chromatid and chromosome breaks including complex rearrangements based on Multiplex FISH and DAPI banding pattern using the SmartType Karyotyper (Digital Scientific, UK).

Organoid and T cell co-culture

Peripheral blood mononuclear cells (PBMCs) and tumor organoids were generated and co-cultured as previously described (39,40). Briefly, PBMCs were isolated from peripheral blood using Ficoll–Paque and cryopreserved for later use. For patient CRC-14, blood was drawn before the first cycle of nivolumab. Culture media for PBMCs was composed of RPMI 1640 (GIBCO), supplemented with 2 mM Ultraglutamine I, 1:100 penicillin/streptomycin and 10% male human AB serum (Sigma-Aldrich; cat. no. H3667) (''T cell medium''). One day before co-culture, PBMCs were thawed in pre-warmed (37°C) T cell medium (human serum was replaced with FCS during thawing) and incubated for 15 min with 25 U/mL benzonase (Merck; cat. no. 70746-3) at 37°C. After washing, cells were resuspended at 2-3 x 10^6 cells/mL in T cell medium supplemented with 150 U/mL IL-2 and cultured overnight at 37°C. 48 hours prior to co-culture, tumor organoids were isolated from Geltrex by incubation with 2 mg/mL dispase II and cultured in CRC medium. Prior to co-culture, tumor organoids (isolated from Geltrex) were stimulated for 24 hours with 200 ng/mL human recombinant IFNγ (Peprotech; cat. no. 300-02). 96-well U-bottom plates were coated with 5 µg/mL anti-CD28 (clone CD28.2, eBioscience; cat. no. 16-0289-81) and kept overnight at 4°C. The next day, tumor organoids were dissociated to single cells with TrypLE Express and resuspended in T cell medium. Anti-CD28-coated plates were washed twice with PBS and PBMC were seeded at a density of 10^5 cells/well and stimulated with single cell dissociated organoids at a 20:1 effector:target ratio. Co-cultures were performed in the presence of 150 U/mL IL-2 and 20 µg/mL anti-PD-1-blocking antibody (kindly donated by Merus, Utrecht; cat. no. 5C4). Half of the medium, including IL-2 and anti-PD-1, was refreshed two to three times per week. Every week, PBMCs were collected, counted, and replated at 10^5 cells/well, and re-stimulated with fresh tumor organoids, for a total of 2 weeks co-culture.

Tumor recognition assay, killing assay, and generation of organoids resistant to autologous reactive T cells

For evaluation of tumor reactivity, 10^5 PBMCs were restimulated with tumor organoids (isolated from Geltrex and stimulated with IFNγ, as described before) at a 2:1 effector: target ratio and seeded in anti-CD28-coated plates in the presence of 20 µg/mL anti-PD-1 and co-cultured for 5 hours for IFNγ evaluation. Golgi-Plug (1:1000, BD; cat. no. 555029) and Golgi-Stop (1:1500, BD, cat. no. 554724) was added after 1 hour and co-culture continued for an additional 4 hours. Cells were washed twice in FACS buffer and stained with the following antibodies: anti-CD3-PerCP-Cy5.5 (BD; cat. no. 332771), anti-CD4-FITC (BD; cat. no. 555346), anti-CD8-BV421 (BD; cat. no. 562429), and near-IR viability dye (Life technologies) for 30 min at 4°C in the dark. Cells were washed twice in FACS buffer, fixed using the Cytofix/Cytoperm kit (BD, according to manufacturer's instructions), and stained for intracellular IFNγ (anti-IFNγ-APC, BD; cat. no. 554702). PBMCs stimulated with 50 ng/mL phorbol 12-myristate 13-acetate (PMA, Sigma-Aldrich; cat. no. 19-144) and 1 mg/mL ionomycin (Sigma-Aldrich; cat. no. I9657) served as positive controls and PBMCs cultured without tumor stimulation as negative controls. Cells were then washed twice with FACS buffer and recorded at a Becton Dickinson Fortessa or LSRII flow cytometer.

For CD137 expression evaluation, 10^5 PBMCs were restimulated with tumor organoids (isolated from geltrex and stimulated with IFNγ, as described before) at a 2:1 effector: target ratio and seeded in anti-CD28-coated plates in the presence of 20 µg/mL anti-PD-1 and co-cultured for 24 hours. Cells were washed twice in FACS buffer and stained with the following antibodies: anti-CD3-PerCP-Cy5.5 (BD), anti-CD4-FITC (BD), anti-CD8-BV421 (BD), anti-CD137-APC (BD; cat. no. 550890) and near-IR viability dye (Life technologies) for 30 min at 4^oC in the dark. PBMCs stimulated with 50 ng/mL phorbol 12-myristate 13-acetate (PMA, Sigma-Aldrich) and 1 µg/mL ionomycin (Sigma-Aldrich) served as positive controls and PBMCs cultured without tumor stimulation as negative controls. Cells were then washed twice with FACS buffer and recorded with a Becton Dickinson Fortessa or LSRII flow cytometer. To determine the sensitivity of tumor organoids to T cell-mediated killing, flat-bottom non-tissue culture-treated plates were coated with 5 mg/mL anti-CD28 and kept at 4°C overnight prior to co-culture. Tumor organoids were previously transduced with luciferase reporter gene. Organoids were isolated from Geltrex 48 hours prior to co-culture and stimulated with 200 ng/mL IFNγ for 24 hours prior to co-culture. The next day, part of the organoids were dissociated to single cells and counted using a hemocytometer. This was used to infer the number of tumor cells per tumor organoid to allow coculture of organoids and T cells at a 5:1 effector:target ratio. Next, tumor organoids were resuspended in the T cell medium. T cells were collected after two weeks of co-culture with tumor organoids and resuspended in the T cell medium. Anti-CD28-coated plates were washed twice with PBS and 1 x 10^4 organoids were seeded for 72 hours in triplicate without T cells or with 5 x 10^4

autologous T cells obtained by two weeks of organoid co-culture. To block MHC class I and II, organoids were pre-incubated for 30 min with 50 µg/mL pan-MHC-I blocking antibody W6/32, or pan-MHC-II blocking antibody T39 (blocking antibody remained present throughout the co-culture; BD; cat no. 555556). At the end of the 72 hours, tumor cells viability in the different conditions was measured by luciferase reporter assay using 3 µg/mL luciferin (Promega; cat. no. E1605). Luminescence was measured with a Tecan reader (1000 ms exposure).

Flow cytometry

For evaluation of MHC-I, tumor organoids were dissociated to single cells using TrypLE Express, with or without overnight pre-incubation with 200 ng/mL IFNγ. Tumor cells were washed in FACS buffer (PBS, 5 mM EDTA, 1% bovine serum antigen) and stained with mouse anti-human HLA-A,B,C-PE (BD Bioscience; cat. no. 555553), or isotype controls (PE mouse IgG1, kappa (BD Bioscience; cat. No 556650) for 30 min at 4°C. Cells were washed twice with FACS buffer and DAPI was added to exclude dead cells prior to recording at a Becton Dickinson Fortessa or LSRII flow cytometer.

AUTHORS CONTRIBUTIONS

Conception and design: Gabriele Picco, Mathew J. Garnett, Alberto Bardelli, Emile Voest

Development of methodology: Gabriele Picco, Chiara Cattaneo, Krijn Dijkstra, Sarah Consonni, Sabrina Arena, Federica di Nicolantonio, Daniele Oddo, Ruby Banerjee.

Acquisition of data (provided animals, acquired and managed patients, provided facilities, etc.): Gabriele Picco, Chiara Cattaneo, Esmée van Vliet, Carlotta Cancelliere, Sara Vieira, Krijn Dijkstra, Iñigo Sánchez Rodríguez, Ruby Banerjee, Luuk Schipper, Andrea Sartore-Bianchi, Salvatore Siena, Federica Di Nicolantonio, Fengtang Yang, Martin Michaelis, Jindrich Cinatl, Sabrina Arena, Cell Model Network UK Group.

Analysis and interpretation of data (e.g., statistical analysis, biostatistics, computational analysis). Gabriele Picco, Chiara Cattaneo, Esmée van Vliet, Giovanni Crisafulli, Giuseppe Rospo, Krijn Dijkstra, Iñigo Sánchez Rodríguez, Daniele Oddo, Sarah Consonni, Ruby Banerjee, Luuk Schipper, Fengtang Yang.

Writing, review, and/or revision of the manuscript: Gabriele Picco, Mathew J. Garnett, Chiara Cattaneo, Esmée van Vliet, Alberto Bardelli, Emile Voest, Sabrina Arena, Federica di Nicolantonio, Krijn Dijkstra.

ACKNOWLEDGMENTS

We thank the Garnett laboratory, Cellular Genetics and Phenotyping facility, and drug screening teams at the Sanger Institute for data generation and assistance. We thank Annalisa Lorenzato (University of Torino) for technical help with sequenom analysis, Pamela Arcella (University of Torino) and Monica Montone (Candiolo Cancer Institute, FPO–IRCCS) for preclinical models establishment. We thank Michael Linnebacher (university of rostock, Germany) for providing the HROC cell models. The M.J.G. laboratory was supported by an SU2C-DCS International Translational Cancer Research Dream Team Grant (SU2C-AACR-DT1213) and the Wellcome Trust Grant 206194. Stand Up To Cancer is a division of the Entertainment Industry Foundation. The SU2C-DCS grant is administered by the American Association for Cancer Research. The research leading to these results has received funding from FONDAZIONE AIRC under 5 per Mille 2018 - ID. 21091 program – P.I. Bardelli Alberto (A.B., F.D.N. and S.S.), AIRC under MFAG 2017 -ID 20236_ P.I. Arena Sabrina (S.A.); H2020 grant agreement no. 635342-2 MoTriColor (A.B.); AIRC IG 2018 - ID. 21923 project (A.B.), AIRC IG n. 17707 and IG n. 21407 (F.D.N.), Therapy in Colorectal Cancer Ministero della Salute, Project n. NET 02352137 (A.S.B., A.B., F.D.N. and S.S.). TRANSCAN-2 JTC 2014 contract no. TRS-2015-00000060 INTRACOLOR (S.A.); FPRC 5xmille 2017 Ministero Salute PTCRC-Intra 2020 (REGENERATION-YIG 2020 project) (S.A.); AIRC-CRUK-FC AECC Accelerator Award contract 22795 (A.B.); Fondazione Piemontese per la Ricerca sul Cancro-ONLUS 5 per mille 2015 Ministero della Salute (A.B. and F.D.N.); Ministero Salute, RC 2019 (A.B. and F.D.N.). Hilfe für krebskranke Kinder Frankfurt e.V., Frankfurter Stiftung für krebskranke Kinder (J.C.). Kent Cancer Trust (M.M.). We thank Kong Xiangjun (Daniel Peeper lab) for providing the B2m-KO virus; and Catrin Lutz (Jos Jonkers lab) for providing the luciferase virus. We thank Arno Velds (NKI) and Shriram Bhosle (Sanger Institute) for bioinformatic support. We thank Matthew Coelho for helpful advice. We thank Cibele Sotero-Caio and Kirsy Roberts (Sanger Institute) for technical help with karyotyping and PCR analysis.

REFERENCES

1. Latham A, Srinivasan P, Kemel Y, Shia J, Bandlamudi C, Mandelker D, et al. Microsatellite Instability Is Associated With the Presence of Lynch Syndrome Pan-Cancer. J Clin Oncol. 2019;37:286–95.

2. Vilar E, Gruber SB. Microsatellite instability in colorectal cancer-the stable evidence. Nat Rev Clin Oncol. 2010;7:153–62.

3. Xie Y-H, Chen Y-X, Fang J-Y. Comprehensive review of targeted therapy for colorectal cancer. Signal Transduct Target Ther. 2020;5:22.

4. Amirouchene-Angelozzi N, Swanton C, Bardelli A. Tumor Evolution as a Therapeutic Target. Cancer Discov. 2017;7;1-13.

5. Misale S, Yaeger R, Hobor S, Scala E, Janakiraman M, Liska D, et al. Emergence of KRAS mutations and acquired resistance to anti-EGFR therapy in colorectal cancer. Nature. 2012;486:532–6.

6. Misale S, Di Nicolantonio F, Sartore-Bianchi A, Siena S, Bardelli A. Resistance to anti-EGFR therapy in colorectal cancer: from heterogeneity to convergent evolution. Cancer Discov. 2014;4:1269–80.

7. Prahallad A, Sun C, Huang S, Di Nicolantonio F, Salazar R, Zecchin D, et al. Unresponsiveness of colon cancer to BRAF(V600E) inhibition through feedback activation of EGFR. Nature. 2012;483:100–3.

8. Corcoran RB, Ebi H, Turke AB, Coffee EM, Nishino M, Cogdill AP, et al. EGFR-mediated re-activation of MAPK signaling contributes to insensitivity of BRAF mutant colorectal cancers to RAF inhibition with vemurafenib. Cancer Discov. 2012;2:227–35.

9. Kopetz S, Grothey A, Yaeger R, Van Cutsem E, Desai J, Yoshino T, et al. Encorafenib, Binimetinib, and Cetuximab in BRAF V600E-Mutated Colorectal Cancer. N Engl J Med. 2019;381:1632–43.

10. Corcoran RB, André T, Atreya CE, Schellens JHM, Yoshino T, Bendell JC, et al. Combined BRAF, EGFR, and MEK Inhibition in Patients with BRAFV600E-Mutant Colorectal Cancer. Cancer Discov. 2018;8:428–43.

11. Oddo D, Sennott EM, Barault L, Valtorta E, Arena S, Cassingena A, et al. Molecular Landscape of Acquired Resistance to Targeted Therapy Combinations in BRAF-Mutant Colorectal Cancer. Cancer Res. 2016;76:4504–15.

12. Hazar-Rethinam M, Kleyman M, Han GC, Liu D, Ahronian LG, Shahzade HA, et al. Convergent Therapeutic Strategies to Overcome the Heterogeneity of Acquired Resistance in BRAFV600E Colorectal Cancer. Cancer Discov. 2018;8:417–27.

13. Pietrantonio F, Oddo D, Gloghini A, Valtorta E, Berenato R, Barault L, et al. MET-Driven Resistance to Dual EGFR and BRAF Blockade May Be Overcome by Switching from EGFR to MET Inhibition in BRAF-Mutated Colorectal Cancer. Cancer Discov. 2016;6:963–71.

14. Cocco E, Benhamida J, Middha S, Zehir A, Mullaney K, Shia J, et al. Colorectal Carcinomas Containing Hypermethylated MLH1 Promoter and Wild-Type BRAF/KRAS Are Enriched for Targetable Kinase Fusions. Cancer Res. 2019;79:1047–53.

15. Pietrantonio F, Di Nicolantonio F, Schrock AB, Lee J, Tejpar S, Sartore-Bianchi A, et al. ALK, ROS1, and NTRK Rearrangements in Metastatic Colorectal Cancer. J Natl Cancer Inst. 2017;109(12).

16. Drilon A, Laetsch TW, Kummar S, DuBois SG, Lassen UN, Demetri GD, et al. Efficacy of Larotrectinib in TRK Fusion-Positive Cancers in Adults and Children. N Engl J Med. 2018;378:731–9.

17. Cocco E, Schram AM, Kulick A, Misale S, Won HH, Yaeger R, et al. Resistance to TRK inhibition mediated by convergent MAPK pathway activation. Nat Med. 2019;25:1422–7.

18. Russo M, Misale S, Wei G, Siravegna G, Crisafulli G, Lazzari L, et al. Acquired Resistance to the TRK Inhibitor Entrectinib in Colorectal Cancer. Cancer Discov. 2016;6:36–44.

19. Misale S, Arena S, Lamba S, Siravegna G, Lallo A, Hobor S, et al. Blockade of EGFR and MEK intercepts heterogeneous mechanisms of acquired resistance to anti-EGFR therapies in colorectal cancer. Sci Transl Med. 2014;6:224ra26.

20. Le DT, Uram JN, Wang H, Bartlett BR, Kemberling H, Eyring AD, et al. PD-1 Blockade in Tumors with Mismatch-Repair Deficiency. N Engl J Med. 2015;372:2509–20.

21. Le DT, Durham JN, Smith KN, Wang H, Bartlett BR, Aulakh LK, et al. Mismatch repair deficiency predicts response of solid tumors to PD-1 blockade. Science. 2017;357:409–13.

22. Overman MJ, Lonardi S, Wong KYM, Lenz H-J, Gelsomino F, Aglietta M, et al. Durable Clinical Benefit With Nivolumab Plus Ipilimumab in DNA Mismatch Repair-Deficient/Microsatellite Instability-High Metastatic Colorectal Cancer. J Clin Oncol. 2018;36:773–9.

23. Le DT, Kim TW, Van Cutsem E, Geva R, Jäger D, Hara H, et al. Phase II Open-Label Study of Pembrolizumab in Treatment-Refractory, Microsatellite Instability-High/Mismatch Repair-Deficient Metastatic Colorectal Cancer: KEYNOTE-164. J Clin Oncol. 2019;JCO1902107.

24. Gurjao C, Liu D, Hofree M, AlDubayan SH, Wakiro I, Su M-J, et al. Intrinsic Resistance to Immune Checkpoint Blockade in a Mismatch Repair-Deficient Colorectal Cancer. Cancer Immunol Res. 2019;7:1230–6.

25. Mandal R, Samstein RM, Lee K-W, Havel JJ, Wang H, Krishna C, et al. Genetic diversity of tumors with mismatch repair deficiency influences anti-PD-1 immunotherapy response. Science. 2019;364:485–91.

26. Hu ZI, Hellmann MD, Wolchok JD, Vyas M, Shia J, Stadler ZK, et al. Acquired resistance to immunotherapy in MMR-D pancreatic cancer. J Immunother Cancer. 2018;6:127.

27. Sahin IH, Akce M, Alese O, Shaib W, Lesinski GB, El-Rayes B, et al. Immune checkpoint inhibitors for the treatment of MSI-H/MMR-D colorectal cancer and a perspective on resistance mechanisms. Br J Cancer. 2019;121:809–18.

28. Chan EM, Shibue T, McFarland JM, Gaeta B, Ghandi M, Dumont N, et al. WRN helicase is a synthetic lethal target in microsatellite unstable cancers. Nature. 2019;568:551–6.

29. Kategaya L, Perumal SK, Hager JH, Belmont LD. Werner Syndrome Helicase Is Required for the Survival of Cancer Cells with Microsatellite Instability. iScience. 2019;13:488–97.

30. Behan FM, Iorio F, Picco G, Gonçalves E, Beaver CM, Migliardi G, et al. Prioritization of cancer therapeutic targets using CRISPR-Cas9 screens. Nature. 2019;568:511–6.

31. Lieb S, Blaha-Ostermann S, Kamper E, Rippka J, Schwarz C, Ehrenhöfer-Wölfer K, et al. Werner syndrome helicase is a selective vulnerability of microsatellite instability-high tumor cells. Elife. 2019;8:e43333

32. Brosh RM Jr. DNA helicases involved in DNA repair and their roles in cancer. Nat Rev Cancer. 2013;13:542–58.

33. Chu WK, Hickson ID. RecQ helicases: multifunctional genome caretakers. Nat Rev Cancer. 2009;9:644–54.

34. van Wietmarschen N, Sridharan S, Nathan WJ, Tubbs A, Chan EM, Callen E, et al. Repeat expansions confer WRN dependence in microsatellite-unstable cancers. Nature. 2020;586:292-298

35. Medico E, Russo M, Picco G, Cancelliere C, Valtorta E, Corti G, et al. The molecular landscape of colorectal cancer cell lines unveils clinically actionable kinase targets. Nat Commun. 2015;6:7002.

36. Picco G, Petti C, Centonze A, Torchiaro E, Crisafulli G, Novara L, et al. Loss of AXIN1 drives acquired resistance to WNT pathway blockade in colorectal cancer cells carrying RSPO3 fusions. EMBO Mol Med. 2017;9:293–303.

37. Lazzari L, Corti G, Picco G, Isella C, Montone M, Arcella P, et al. Patient-Derived Xenografts and Matched Cell Lines Identify Pharmacogenomic Vulnerabilities in Colorectal Cancer. Clin Cancer Res. 2019;25:6243–59.

38. Arena S, Bellosillo B, Siravegna G, Martínez A, Cañadas I, Lazzari L, et al. Emergence of Multiple EGFR Extracellular Mutations during Cetuximab Treatment in Colorectal Cancer. Clin Cancer Res. 2015;21:2157–66.

39. Dijkstra KK, Cattaneo CM, Weeber F, Chalabi M, van de Haar J, Fanchi LF, et al. Generation of Tumor-Reactive T Cells by Co-culture of Peripheral Blood Lymphocytes and Tumor Organoids. Cell. 2018;174:1586–98.e12.

40. Cattaneo CM, Dijkstra KK, Fanchi LF, Kelderman S, Kaing S, van Rooij N, et al. Tumor organoid-T-cell coculture systems. Nat Protoc. 2020;15:15–39.

41. Schoenfeld AJ, Hellmann MD. Acquired Resistance to Immune Checkpoint Inhibitors. Cancer Cell. 2020;37:443–55.

42. Schrock AB, Ouyang C, Sandhu J, Sokol E, Jin D, Ross JS, et al. Tumor mutational burden is predictive of response to immune checkpoint inhibitors in MSI-high metastatic colorectal cancer. Ann Oncol. 2019;30:1096–103.

43. Germano G, Lamba S, Rospo G, Barault L, Magrì A, Maione F, et al. Inactivation of DNA repair triggers neoantigen generation and impairs tumour growth. Nature. 2017;552:116–20.

44. Langer CJ, Gadgeel SM, Borghaei H, Papadimitrakopoulou VA, Patnaik A, Powell SF, et al. Carboplatin and pemetrexed with or without pembrolizumab for advanced, non-

squamous non-small-cell lung cancer: a randomised, phase 2 cohort of the open-label KEYNOTE-021 study. Lancet Oncol. 2016;17:1497–508.

45. Rosenthal R, Cadieux EL, Salgado R, Bakir MA, Moore DA, Hiley CT, et al. Neoantigen-directed immune escape in lung cancer evolution. Nature. 2019;567:479–85.

46. Aggarwal M, Sommers JA, Shoemaker RH, Brosh RM Jr. Inhibition of helicase activity by a small molecule impairs Werner syndrome helicase (WRN) function in the cellular response to DNA damage or replication stress. Proc Natl Acad Sci U S A. 2011;108:1525–30.

47. Aggarwal M, Banerjee T, Sommers JA, Iannascoli C, Pichierri P, Shoemaker RH, et al. Werner syndrome helicase has a critical role in DNA damage responses in the absence of a functional fanconi anemia pathway. Cancer Res. 2013;73:5497–507.

48. Bou-Hanna C, Jarry A, Lode L, Schmitz I, Schulze-Osthoff K, Kury S, et al. Acute cytotoxicity of MIRA-1/NSC19630, a mutant p53-reactivating small molecule, against human normal and cancer cells via a caspase-9-dependent apoptosis. Cancer Lett. 2015;359:211–7.

49. van der Meer D, Barthorpe S, Yang W, Lightfoot H, Hall C, Gilbert J, et al. Cell Model Passports-a hub for clinical, genetic and functional datasets of preclinical cancer models. Nucleic Acids Res. 2019;47:D923–9.

50. Russo M, Lamba S, Lorenzato A, Sogari A, Corti G, Rospo G, et al. Reliance upon ancestral mutations is maintained in colorectal cancers that heterogeneously evolve during targeted therapies. Nat Commun. Nature Publishing Group; 2018;9:1–12.

51. Whitehead RH, Macrae FA, St John DJ, Ma J. A colon cancer cell line (LIM1215) derived from a patient with inherited nonpolyposis colorectal cancer. J Natl Cancer Inst. 1985;74:759–65.

52. Iorio F, Knijnenburg TA, Vis DJ, Bignell GR, Menden MP, Schubert M, et al. A Landscape of Pharmacogenomic Interactions in Cancer. Cell. 2016;166:740–54.

53. Garnett MJ, Edelman EJ, Heidorn SJ, Greenman CD, Dastur A, Lau KW, et al. Systematic identification of genomic markers of drug sensitivity in cancer cells. Nature. 2012;483:570–5.

54. Michaelis M, Wass MN, Cinatl J. Drug-adapted cancer cell lines as preclinical models of acquired resistance. Cancer Drug Resistance Cancer Drug Resist. 2019;2:447-456

55. Michaelis M, Rothweiler F, Barth S, Cinatl J, van Rikxoort M, Löschmann N, et al. Adaptation of cancer cells from different entities to the MDM2 inhibitor nutlin-3 results in the emergence of p53-mutated multi-drug-resistant cancer cells. Cell Death Dis. 2011;2:e243.

56. Rospo G, Lorenzato A, Amirouchene-Angelozzi N, Magrì A, Cancelliere C, Corti G, et al. Evolving neoantigen profiles in colorectal cancers with DNA repair defects. Genome Med. 2019;11:42.

57. Corti G, Bartolini A, Crisafulli G, Novara L, Rospo G, Montone M, et al. A Genomic Analysis Workflow for Colorectal Cancer Precision Oncology. Clin Colorectal Cancer. 2019;18:91–101.e3.

58. Crisafulli G, Mussolin B, Cassingena A, Montone M, Bartolini A, Barault L, et al. Whole

exome sequencing analysis of urine trans-renal tumour DNA in metastatic colorectal cancer patients. ESMO Open. 2019;4:e000572.

59. Garcia-Alonso L, Iorio F, Matchan A, Fonseca N, Jaaks P, Peat G, et al. Transcription Factor Activities Enhance Markers of Drug Sensitivity in Cancer. Cancer Res. 2018;78:769–80.

60. Roumeliotis TI, Williams SP, Gonçalves E, Alsinet C, Del Castillo Velasco-Herrera M, Aben N, et al. Genomic Determinants of Protein Abundance Variation in Colorectal Cancer Cells. Cell Rep. 2017;20:2201–14.

61. Nusinow DP, Szpyt J, Ghandi M, Rose CM, McDonald ER 3rd, Kalocsay M, et al. Quantitative Proteomics of the Cancer Cell Line Encyclopedia. Cell. 2020;180:387–402.e16.

62. Pacini C, Dempster JM, Boyle I, Gonçalves E, Najgebauer H, Karakoc E, et al. Integrated cross-study datasets of genetic dependencies in cancer. Nat Commun. 2021;12:1661.

63. Hinrichs AS, Karolchik D, Baertsch R, Barber GP, Bejerano G, Clawson H, et al. The UCSC Genome Browser Database: update 2006. Nucleic Acids Res. 2006;34:D590–8.

64. Picco G, Chen ED, Alonso LG, Behan FM, Gonçalves E, Bignell G, et al. Functional linkage of gene fusions to cancer cell fitness assessed by pharmacological and CRISPR-Cas9 screening. Nat Commun. 2019;10:2198.

FIGURE LEGENDS

Figure 1: Landscape of WRN dependency in dMMR CRC preclinical models. ***A****, Oncoprint representation of WRN dependency and oncogenic driver mutations in dMMR CRC models. For each model, WRN dependency status, type of model, tumor type, mutational burden, model type, publication status of WRN dependency data, and assay types are annotated. Missense mutations in KRAS and BRAF, and oncogenic rearrangements in NTRK1, ALK, and RSPO3 are indicated.* ***B****, WRN depletion assay in 29 dMMR CRC cell lines. Bars are normalized viability upon siRNA-mediated WRN depletion in WRN-dependent cell lines and WRN-independent cell lines, as indicated. Non-targeting siRNA or PLK1 siRNAs (blue bars) were used as negative and positive controls, respectively. Dots represent mean and SD of 3 independent experiments with 5 technical replicates each. SNU1040 was tested twice.* ***C****, WRN dependency in hard to transfect cell lines and models displaying an intermediate response by RNA interference evaluated by CRISPR-cas9-based clonogenic assays (14 days).* ***D****, Clonogenic assays of dMMR CRC models insensitive to WRN knockout. Clonogenic assays are representative of three independent experiments.* ***E****, Genomic and proteomic profile of MMR-pathway gene alterations in dMMR CRC cancer models. Coloured (red, blue, green, and light black) boxes indicate the presence of the alteration. Light grey boxes represent data unavailable.*

Figure 2. WRN dependence in models of acquired resistance to targeted agents. ***A****, Representation of in vitro dMMR CRC models of acquired resistance to EGFR, NTRK1, and BRAF-target therapies.* ***B,*** *Cell viability in models of acquired resistance upon transfection of WRN-targeting siRNAs. PLK1 (siPLK1) siRNA were used as positive control. MMR-proficient (pMMR) cell line SW620 was included as a negative control. Data are the mean ± standard deviation (SD) of three independent experiments with five technical replicate each and were analyzed with two-tailed Student's t-test comparing siWRN to non-targeting control: ns, not significant; * p ≤0.05, ** p ≤0.01 and *** p ≤0.001.* ***C****, Normalized viability data in models of acquired resistance upon WRN knockout. Non-essential (sgNon) and PLK1 (sgPLK1) sgRNAs were used as negative and positive controls, respectively. The pMMR SW620 cell line was a negative control. Data are mean and SD of 3 independent experiments with 5 technical replicates each. Statistical significance was evaluated comparing WRN sgRNAs versus non-essential gene sgRNA (sgNon) performing a two-tailed Student's t-test: ns, not significant; P ≤0.05, ** P ≤0.01 and *** P≤0.001.* ***D,*** *Viability of IRCC-1-XL-ENT-R cells upon transfection of WRN-targeting siRNAs.* ***E****, Normalized viability data of IRCC-1-XL-ENT-R cells upon WRN knockout.* ***F****, WRN reduction verified by Western blot. siRNA non-targeting controls (siNTC), siRNA targeting WRN (siWRN). Tubulin is a loading control. Representative of two independent experiments.* ***G****, Quantification of metaphase chromatid breaks in IRCC1-XL-ENTR-R cells 96h after transduction with WRN sgRNA (n ≥ 20 randomly selected metaphases analyzed).* ***H****, Representative metaphase karyotype of IRCC-1-XL-ENT-R cells after 96h transduction with WRN-targeting sgRNA2. Red arrows indicate chromosome (chrb) and chromatid (chtb) breaks.*

Figure 3. WRN dependency in chemo-resistant dMMR/MSI-H CRC sublines and patient-derived model. ***A****, dMMR CRC models of acquired resistance to chemotherapeutic agents.* ***B,*** *Proliferation assays of cell line models of acquired resistance to chemotherapies and parental counterparts. Data are average ± SD of three technical replicates and are representative of three independent experiments.* ***C,*** *The IRCC-114-XL cell line established from a PDX model of a Lynch*

syndrome patient treated with mFOLFOX for 6 months after surgery. **D**, *Computed tomography (CT) scan of the IRCC-114 patient displaying drug resistance and early tumor progression after chemotherapy.* ***E, F, G,*** *Normalized viability of upon siRNA-mediated WRN depletion in HCT116 and SW48 chemotherapy-resistant sublines and IRCC-114-XL cells. Non-targeting siRNA (siNT) and siPLK1 were used as negative and positive controls, respectively. Data are mean and SD of 3 independent experiments with 5 technical replicates each. Statistical significance was evaluated using a Student's t-test: ns, not significant; * P ≤0.05, ** P ≤0.01 and *** P≤0.001* **H**, *Normalized viability for IRCC-114-XL cells upon WRN knockout. Non-essential (sgNon) and PLK1 (sgPLK1) sgRNAs were negative and positive controls, respectively. Data are mean and SD of 2 independent experiments with 5 technical replicates each. Statistical significance was calculated using a two-tailed Student's t-test: ns, not significant; P ≤0.05, ** P ≤0.01, and *** P≤0.001.* **I**, *Chromosome breaks in IRCC-114-XL cell line 96h after WRN depletion (≥20 metaphase spreads assayed).* **J**, *Representative images of IRCC-114-XL metaphases (left) and a pulverized metaphase (right) after 96h of transduction with a sgWRN. Red arrows indicate chromosome (chrb) and chromatid (chtb) breaks.*

Figure 4. ***Patient-derived CRC dMMR organoid models refractory to immunotherapy are WRN dependent.*** **A**, *dMMR CRC tumor organoid-T cell co-cultures from a sporadic dMMR primary tumor (left panel) or two lesions in a patient with a heterogeneous clinical response to nivolumab (right panel).* ***B****, CD137 expression of CD8+ T cells upon stimulation with different CRC-12-derived organoids lines. Values are background corrected, and bars represent mean and SEM of two independent experiments.* ***C****, Organoid killing after 3 days of T cell co-culture. Error bars represent SEM of at least two biological replicates.* ***D****, Viability in CRC-12 and CRC-12-RES upon WRN knockout. Non-essential (sgNon) and PLK1 (sgPLK1) sgRNAs were negative and positive controls, respectively. Data are the mean ± standard deviation (SD) of three independent experiments with 6 technical replicates each.* ***E****, Computer tomography scans over an 8-month period of the peritoneal metastasis lesion and the primary tumor of CRC-14 patient treated with nivolumab. Red and green arrow indicates a size increase and reduction, respectively.* ***F****, IFNγ expression of CD8+ T cells upon exposure to CRC-14a (responsive) or CRC-14b (non responsive) organoids. Stimulation with PMA/ionomycin is a positive control. Background IFN-γ-positive cells (in unstimulated condition) was subtracted from the signal. Data are the mean and SEM of at least 2 independent experiments.* ***G****, Viability of CRC-14b organoids upon WRN knockout. sgNon and sgPLK1 were used as negative and positive controls, respectively. Data are the mean ± standard deviation (SD) of four independent experiments (10 technical replicates each).* ***H****, Representative images of CRC-14b (10x magnification) 10 days after transduction with indicated sgRNAs.* ***C****,* ***D****,* ***G****: Significance was evaluated by two-tailed Student's t test. ns, not significant; ** P ≤0.01 and *** P≤0.001.*

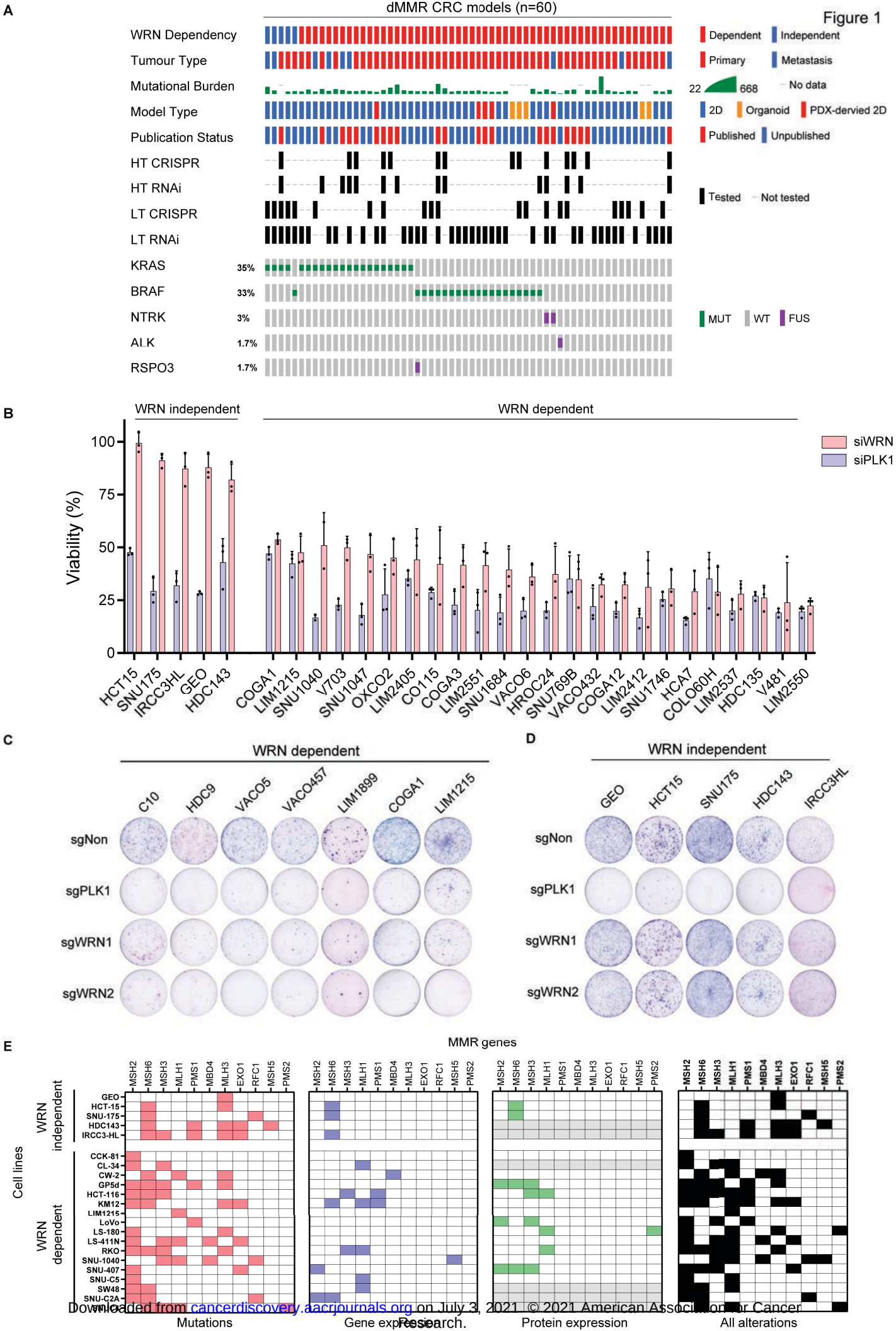

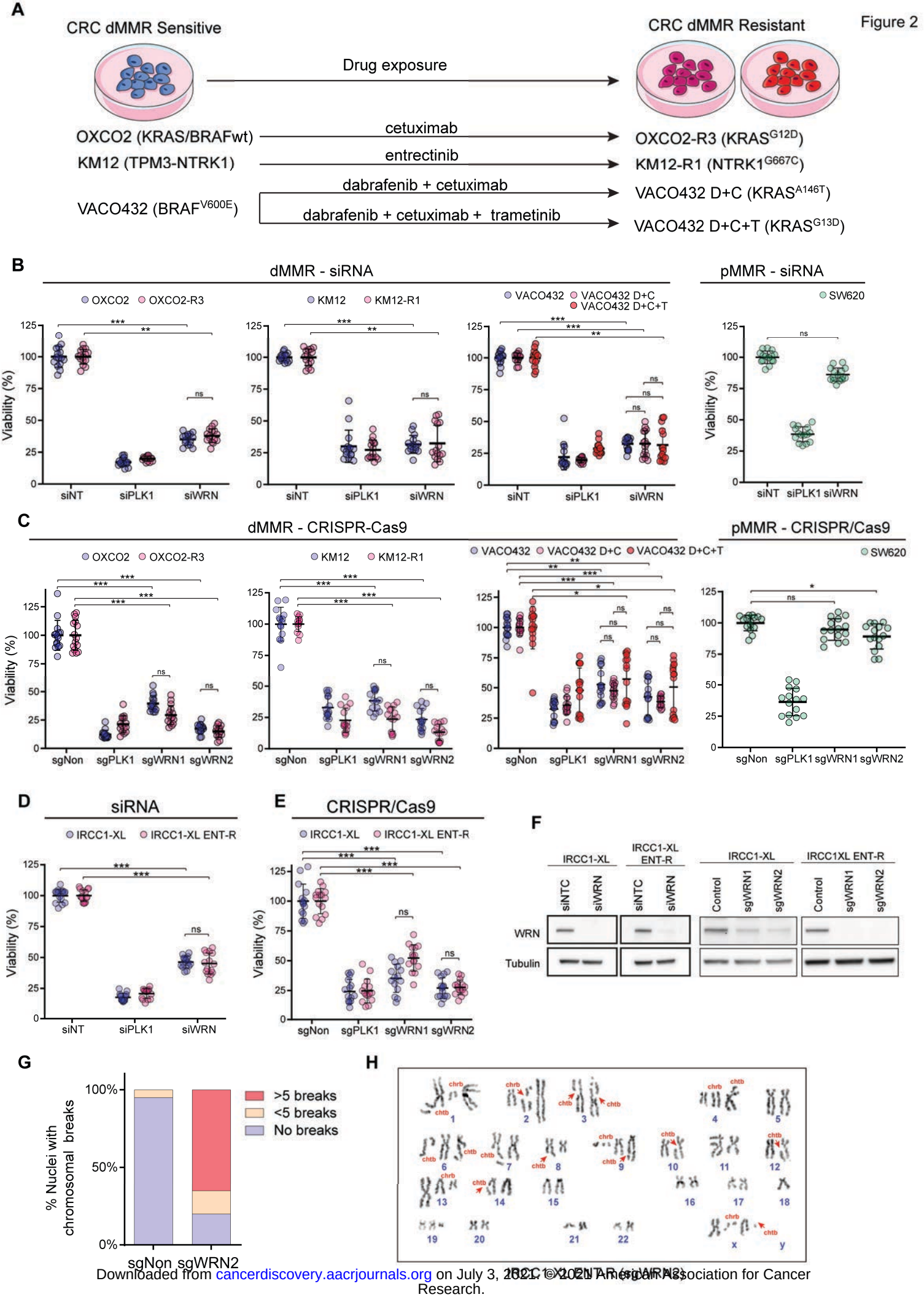

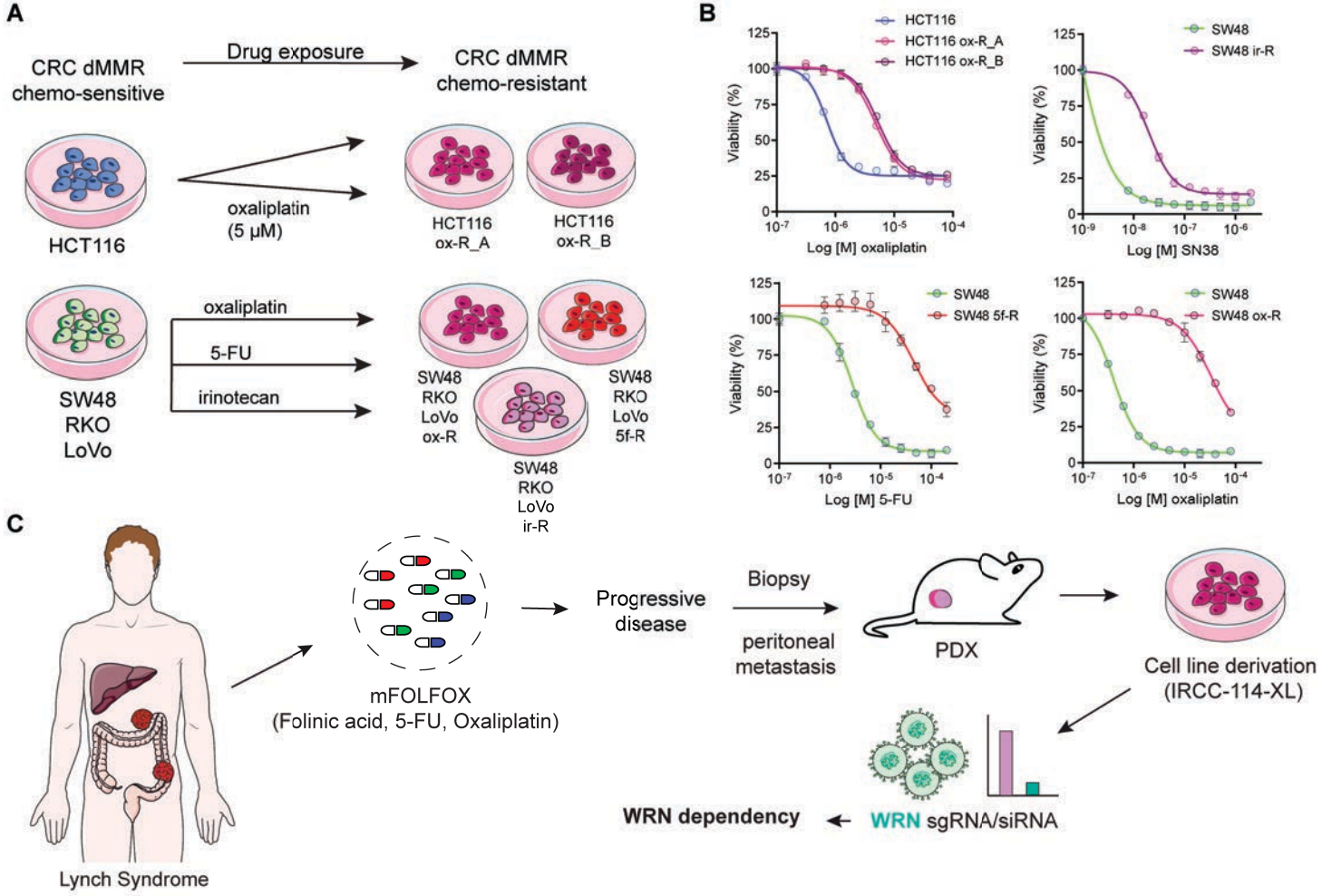

Figure 3

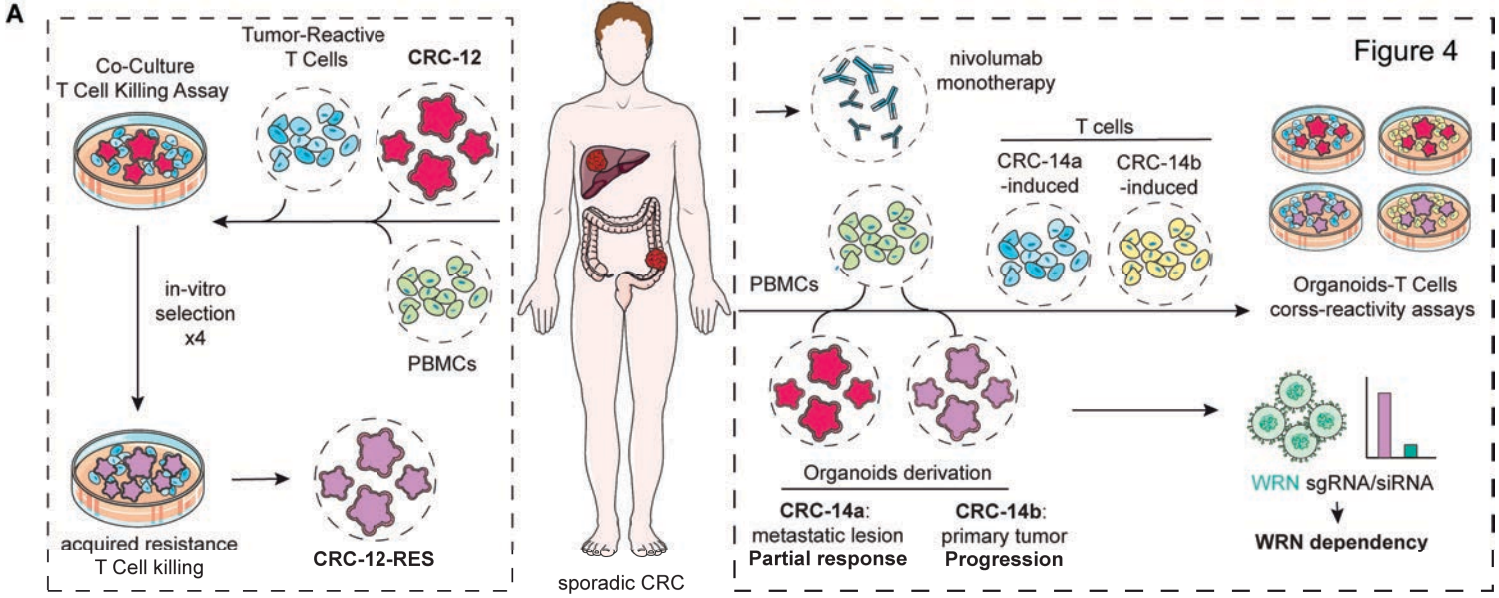

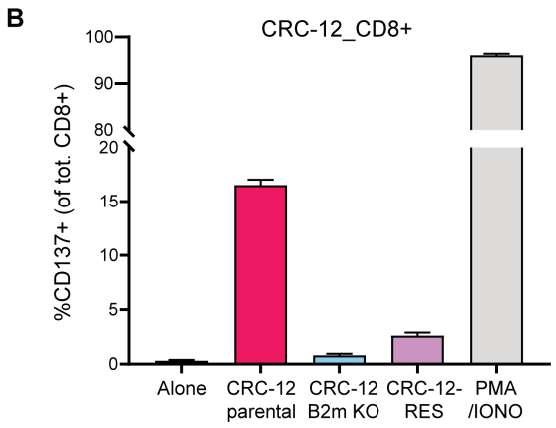

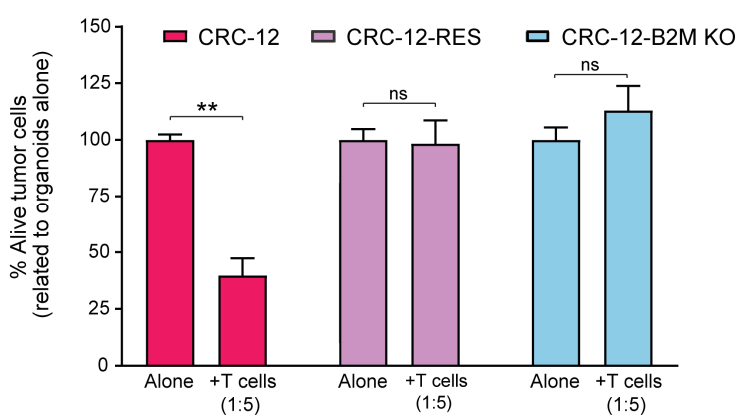

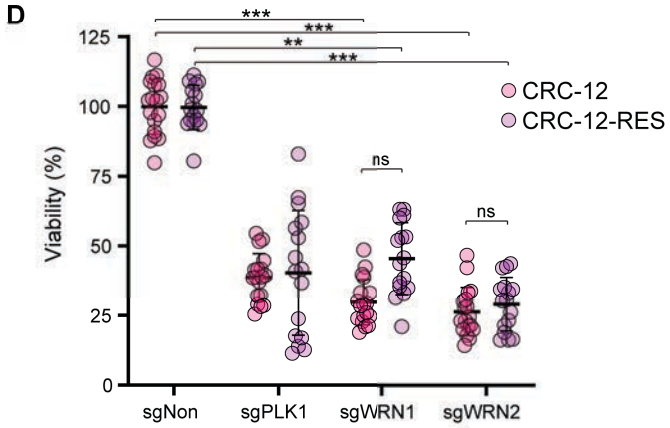

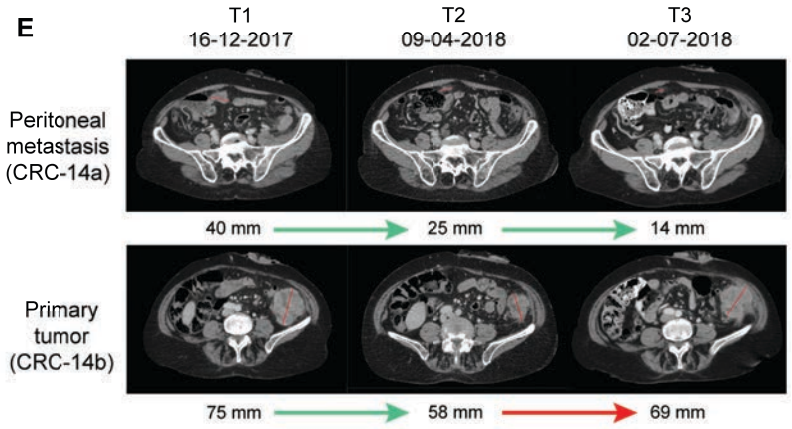

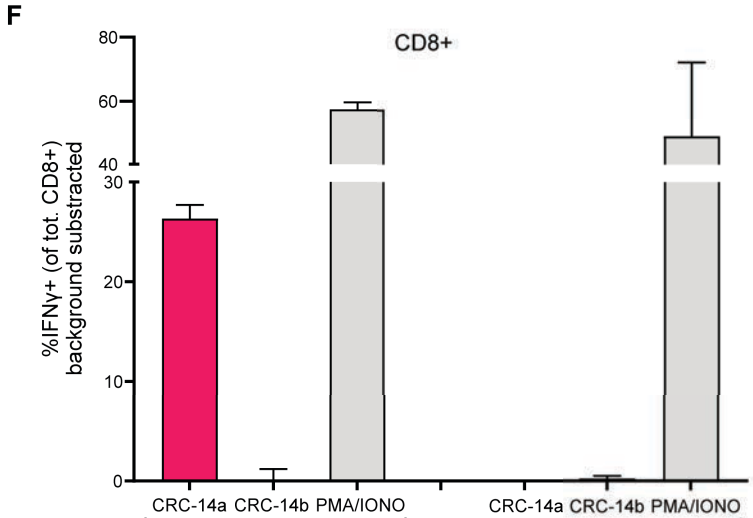

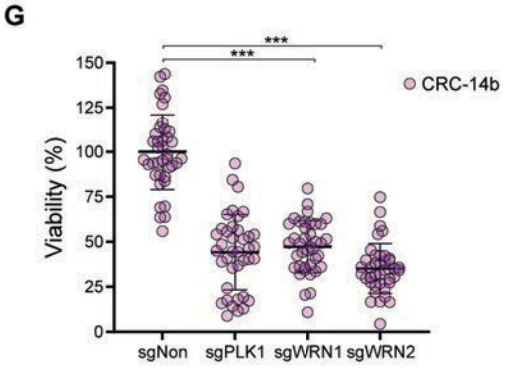

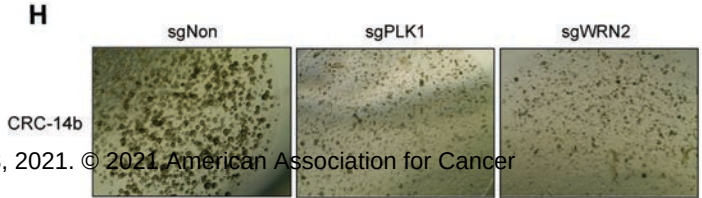

AACR American Association for Cancer Research

CANCER DISCOVERY

Werner helicase is a synthetic-lethal vulnerability in Mismatch Repair-Deficient Colorectal Cancer Refractory to Targeted Therapies, Chemotherapy and Immunotherapy

Gabriele Picco, Chiara Maria Cattaneo, Esmee J. van Vliet, et al.

Cancer Discov Published OnlineFirst April 9, 2021.